

Anomalous magnetic behavior of Ba₂CoO₄ with isolated CoO₄ tetrahedra

Qiang Zhang,^{1,2} Guixin Cao,¹ Feng Ye,² Huibo Cao,² Masaaki Matsuda,² D. A. Tennant,² Songxue Chi,² S. E. Nagler,² W. A. Shelton,³ Rongying Jin,¹ E. W. Plummer,¹ and Jiandi Zhang^{1,*}

¹*Department of Physics and Astronomy, Louisiana State University, Baton Rouge, Louisiana 70803, USA*

²*Neutron Scattering Division, Oak Ridge National Laboratory, Oak Ridge, Tennessee 37831, USA*

³*Cain Department of Chemical Engineering, Louisiana State University, Baton Rouge, Louisiana 70803, USA*



(Received 8 September 2018; published 14 March 2019)

The dimensionality of the electronic and magnetic structure of a given material is generally predetermined by its crystal structure. Here, using elastic and inelastic neutron scattering combined with magnetization measurements, we find unusual magnetic behavior in three-dimensional (3D) Ba₂CoO₄. In spite of isolated CoO₄ tetrahedra, the system exhibits a 3D noncollinear antiferromagnetic order in the ground state with an anomalously large Curie-Weiss temperature of 110 K compared to $T_N = 26$ K. More unexpectedly, spin dynamics displays quasi-two-dimensional spin-wave dispersion with an unusually large spin gap, and one-dimensional magnetoelastic coupling. Our results indicate that Ba₂CoO₄ is a unique system for exploring the interplay between isolated polyhedra, low-dimensional magnetism, and spin states in oxides.

DOI: [10.1103/PhysRevB.99.094416](https://doi.org/10.1103/PhysRevB.99.094416)

I. INTRODUCTION

It is anticipated that low-dimensional magnetism in a material is directly related to its low-dimensional crystal structure [1], such as in cuprates [2], Fe-based pnictides [3], ferromagnetic semiconductor CrSiTe₃ [4], double-layer perovskite Sr₃(Ru_{1-x}Mn_x)₂O₇ [5], or Weyl semimetal YbMnBi₂ [6], etc. In these materials, the quasi-two-dimensional (2D) magnetism originates from the clearly layered crystal structure where the nearest-neighbor (NN) M - M distance (where M is a transition-metal element) along the interlayer direction is much larger than that within the layer, which yields a very weak interlayer magnetic interaction [1–6]. It would be of great interest to explore whether quasi-2D magnetism could be realized in a nonlayered compound involving comparable NN M - M distances in a crystallographically three-dimensional (3D) system. The identification of such a system may shed light on the microscopic origin of quasi-2D magnetism.

Different from other well-studied cobaltates with the Co ion in an octahedral environment, monoclinic Ba₂CoO₄ [7,8] has a 3D crystallographic structure with *isolated* tetrahedral CoO₄ without any corner-, edge-, or face sharing [Fig. 1(a)]. Naively one would expect that the spin correlation in Ba₂CoO₄ is very weak, presumably dictated by spin dipole-dipole interaction with energy $U \approx \frac{1}{(137)^2} \left(\frac{g\mu_B}{4}\right)^3 \text{Ry}$ [9]. Using the shortest Co-Co distance of 4.67 Å, we estimate $U \sim 0.01$ meV, implying that any magnetic ordering would happen below 0.1 K. Yet, Ba₂CoO₄ exhibits antiferromagnetic (AFM) ground state below $T_N \approx 26$ K [8,10,11] with an anomalously high Curie-Weiss temperature ($|\theta| \sim 110$ K), which is > 4 times larger than T_N [11]. The large $|\theta|/T_N$ ratio could be a result of spin frustration [12,13] or low-dimensional magnetism [14] existing in the system. To

complicate any interpretation of magnetism is the fact that the reported magnetic structures are inconsistent with each other [10,15]. Boulahya *et al.* [10] reported a canted AFM order in the bc plane based on powder neutron-diffraction measurements. In contrast, muon spin rotation and relaxation (μ^+ SR) experiments [15] found that the magnetic moment is basically along the a axis. In addition, spin dimer analysis [16] for the magnetic coupling in Ba₂CoO₄ has no indication of quasi-2D magnetism. Super-superexchange (SSE) mechanism [16–19], which describes spin interactions beyond direct Co-O-Co superexchange pathways, was proposed to be responsible for the magnetic interaction in Ba₂CoO₄. However, there is no experimental confirmation to date.

Here, we demonstrate different dimensionality between static and dynamical magnetism in Ba₂CoO₄. The system exhibits a 3D noncollinear AFM order with buckled zigzag chains along the b axis below $T_N = 26$ K but one-dimensional (1D) magnetoelastic coupling occurs along the a direction, despite well-separated CoO₄ tetrahedra [Fig. 1(a)]. However, the spin waves (SWs) display a quasi-2D character with dispersion in the ab plane. An anomalous spin gap (~ 2.55 meV) comparable to the SW bandwidth reflects a large magnetic anisotropy. The magnon dispersion relation analyzed using the linear SW theory reveals large anisotropic magnetic interactions. The results can be interpreted in terms of a frustrated network of Co-O \cdots O-Co spin-exchange pathways where the overlapping oxygen p orbitals determine the amplitude of magnetic interactions. The uniaxial magnetoelastic effect is the evidence of a certain spin-lattice coupling to stabilize the 3D AFM order against the spin frustration.

II. RESULTS AND DISCUSSION

Ba₂CoO₄ crystals were synthesized using the floating-zone method (See Supplemental Material [20]). Single-crystal neutron diffraction was used to determine the structure of

*jiandiz@lsu.edu

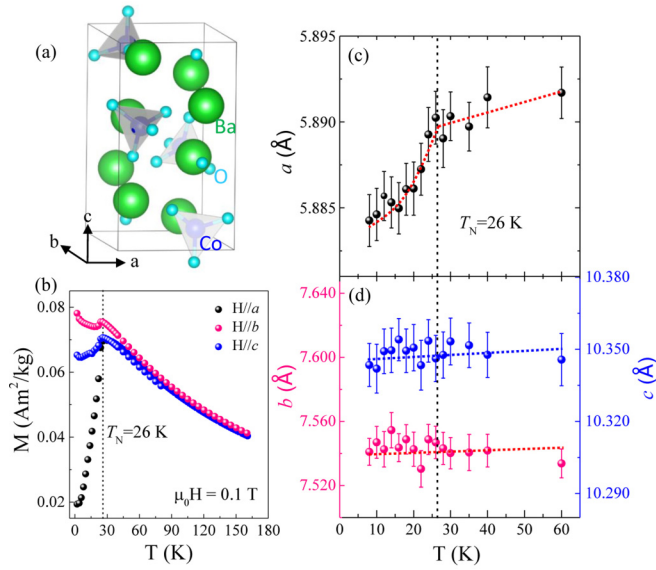


FIG. 1. Structural information of Ba_2CoO_4 . (a) A 3D view of the monoclinic unit cell for $\text{Ba}_8\text{Co}_4\text{O}_{16}$ (simplified as Ba_2CoO_4). (b) T dependence of the magnetization curves for Ba_2CoO_4 in a field of 0.1 T applied parallel to the crystalline a -, b -, and c axes. (c), (d) T dependence of the lattice constants a , b , and c . The vertical dashed line shows the location of AFM transition temperature T_N .

Ba_2CoO_4 [21,22], revealing a monoclinic structure with space group $P2_1/n$ (No. 14) at 5 K as illustrated in Fig. 1(a). There are 4 Co atoms in one crystalline unit cell. This result is consistent with previous neutron- and x-ray-diffraction measurements [10,11]. Temperature (T) dependence of the magnetization (M) for Ba_2CoO_4 in a field of 0.1 T is shown in Fig. 1(b) for three principal directions. Note that M decreases with increasing temperature above T_N with no anisotropy. Below $T_N = 26$ K, M_a drops much faster than M_c , while M_b increases after a small drop. This indicates anisotropic magnetism below T_N , with the AFM configuration along both the a and c directions, but ferromagnetic (FM)-like alignment along the b direction. The rapid decrease of M_a below T_N implies that the moment direction mainly points to the a axis. Fitting to the inverse susceptibility ($H//a$) at the high-temperature linear portion of the curve with the Curie-Weiss law ($\chi = \frac{C}{T+\theta}$) yields a Curie-Weiss temperature $\theta \approx 109$ K, consistent with the previous reports [10,11].

Figures 1(c) and 1(d) show the temperature dependences of the lattice constants determined by measuring the Q scans through the nuclear peaks (400), (020), and (004) of neutron diffraction, given there is a negligible change in the monoclinic beta angle $< 0.6^\circ$ between RT and 5 K. Above T_N , the lattice constants in all three directions show identical T dependence with thermal expansion coefficient $\alpha \sim 9 \times 10^{-6} \text{ K}^{-1}$ (close to the value for glass of $7.6 \times 10^{-6} \text{ K}^{-1}$ [23]). However, the lattice constant a exhibits anomalous behavior with an abrupt and nonlinear drop below T_N , indicating strong magnetoelastic coupling in this specific direction. The T dependence of the lattice constant a [Fig. 1(c)] scales inversely with the magnetic order parameter shown in Fig. 2(a).

Magnetic peaks with a commensurate propagation wave vector $\mathbf{k} = (-1/2, 0, 1/2)$ appear below T_N in the neutron

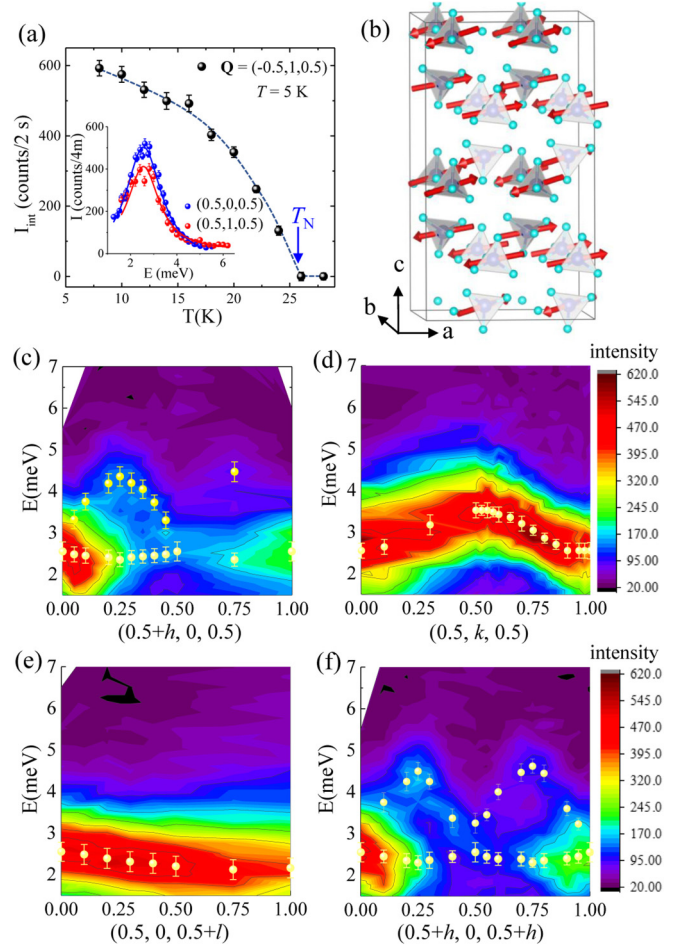


FIG. 2. (a) Order parameter of magnetic $(-0.5, 1, 0.5)$ peak. The inset shows the spin gap at two magnetic zone centers $(0.5, 0, 0.5)$ and $(0.5, 1, 0.5)$. (b) The 3D graphic representation of the determined magnetic structure of Ba_2CoO_4 at 5 K within $2a \times 1.3b \times 2c$ unit cells (note that one magnetic unit cell is $2a \times b \times 2c$ unit cells). (c)–(f) Experimental $S(Q, E)$ contour plots along the $[H00]$, $[0K0]$, $[00L]$, and $[H0H]$ directions in the reciprocal lattice units (r.l.u.). The dot symbols show the experimental spin-wave dispersions obtained by the fits to the raw data (see details in the main text).

diffraction due to long-range magnetic ordering. The T -dependent peak intensity of the magnetic Bragg peak $(-1/2, 1, 1/2)$ in Fig. 2(a) shows an AFM transition at T_N . As illustrated in Fig. 2(b), the overall magnetic structure is AFM with an ordered moment of $2.69(4) \mu_B/\text{Co}$, consisting of 16 Co spins in the magnetic unit cell. The magnetic unit cell is $2a \times b \times 2c$ with respect to the crystalline unit cell with $|\mathbf{m}_a| = 2.377 \mu_B$, $|\mathbf{m}_b| = 1.128 \mu_B$, and $|\mathbf{m}_c| = 0.586 \mu_B$, respectively. All the Co spins are antiparallel along the a and c axes but have a double-stripe-type parallel configuration along the b axis, consistent with the magnetization measurements. The moments primarily point along the a axis and alternatively canted with a canting angle to the b axis $\sim \pm 25^\circ$ and to the c axis $\sim \pm 13^\circ$ [21,24,25].

The spin dynamics is investigated using inelastic neutron scattering. The inset of Fig. 2(a) shows the spectra of the constant- Q energy scan at two magnetic zone centers, $(1/2,$

TABLE I. Optimal parameters obtained by fitting experimental SW dispersions with the linear spin-wave theory (see details in the main text), compared with corresponding Co-Co distances.

	SJ_1	SJ_1'	SJ_2	SJ_2'	SJ_{\perp}	SJ_3	SA_a	SA_b	SA_c
Value (meV)	1.29(6)	1.13(4)	0.58(6)	0.45(4)	0.015(8)	1.11(5)	0.5×10^{-3}	0.52(8)	0.46(7)
Co-Co distance (Å)	4.662	5.323	4.797	5.442	5.186	5.884			

0, 1/2) and (1/2, 1, 1/2) at 5 K. A spin gap of $\Delta \approx 2.55(3)$ meV is observed at 5 K and disappears at T_N , confirming its magnetic origin. This is in stark contrast to the isotropic nature of the high spin state Co⁴⁺ ($S = 5/2$, $L = 0$, $e^2t_2^3$) reported previously [7,8,10,11,15] due to the full quenching of the orbital angular momentum and consequently the absence of strong spin gap. The AFM ordered moment of $2.69(4)\mu_B$ is also much lower than $5\mu_B$ expected for high spin state of Co⁴⁺ but close to $3\mu_B$ for the intermediate spin state of Co⁴⁺ ($S = 3/2$). Both indicate that the ground state of Ba₂CoO₄ is in the intermediate spin (IS) state Co⁴⁺ ($S = 3/2$, $L \neq 0$, $e^3t_2^2$). While the IS state of Co⁴⁺ was frequently observed in cobaltites when Co is in an octahedral environment, the IS state of Co⁴⁺ in the tetrahedral environment seems very rare. Early theoretical calculations [26] indicated that all the IS ($S = 3/2$) states of $3d^5$ cation in the tetrahedral environment may not be stable. Recently, Kauffmann *et al.* [27] proposed that the off-centering of O atoms from their ideal tetrahedral positions may induce the intermediate spin state of tetrahedral Co⁴⁺ ion. The x-ray-absorption spectroscopy and/or theoretical calculations are needed in order to investigate the microscopic origin of the possible IS state in Ba₂CoO₄.

Figures 2(c)–2(f) display the contour plots of $S(Q, E)$, determined from the constant- Q energy scans along the $[H 0 0]$, $[0 K 0]$, $[0 0 L]$, and diagonal $[H 0 H]$ direction at 5 K (see Note 3 in Supplemental Material [28]). Two SW branches appear along the $[H 0 0]$ and $[H 0 H]$ directions with the more dispersive being the high-energy branch. These two branches nearly merge along the $[0 K 0]$ and $[0 0 L]$ directions. Surprisingly, the magnon bandwidth is less than 3 meV, close to the spin-gap value of ~ 2.6 meV. In contrast, both the energy and intensity of the SW along the $[0 0 L]$ direction show negligible dispersion, indicating that Ba₂CoO₄ exhibits a surprising quasi-2D magnetism.

To identify the observed SW modes and quantitatively obtain the magnetic exchange parameters, we have performed the linear SW calculations using the SPINW package [29] with an effective Heisenberg-like Hamiltonian given by

$$H = \sum_{i \neq j} J_{ij} \vec{S}_i \cdot \vec{S}_j + \sum_i A_i \vec{S}_i^2, \quad (1)$$

where \vec{S}_i denotes the spin of magnetic Co ion at site i , J_{ij} describes the magnetic exchange-coupling constant between spin pairs at site i and j , $\sum_{i \neq j}$ indicates summation over pairs of spins, and A_i is the diagonal element of the 3×3 single-ion anisotropy matrix. The best-fitting values of the exchange parameters SJ_{ij} and anisotropy parameter SA are listed in Table I. Compared to SA_b and SA_c , the anisotropy parameter SA_a is extremely small, consistent with the ordered moment mainly aligned to the a axis. Due to the large spin gap, it is impossible to fit the experimental data of spin waves without large anisotropy term. It is worthwhile noting that the

spin dimer analysis proposed in Ref. [16] does not include single-ion anisotropy.

Figure 3(a) illustrates the magnetic structure, doubling of the ab plenary lattice structure (PLS), and the important exchange constants used in the fitting of spin waves. Considering only Co sites for two stacking PLSs shown in Fig. 3(a), each Co atom is surrounded by 6 NN Co atoms with comparable Co-Co distances. The two adjacent PLSs are not identical, thus there are two quasi-2D PLSs in the magnetic unit cell alternating along the c axis and connected by the exchange coupling of J_{\perp} . Figure 3(b) shows the projection of one quasi-2D PLS onto the ab plane. The spin configuration within each PLS is collinear but the spin ordering between the adjacent PLSs is not, forming an overall noncollinear AFM order. For each quasi-2D PLS, the spins form a buckled AFM double-chain structure with strong exchange couplings [J_1 , and J_1' , see Fig. 3(b)] along the b direction. Six NN pairs (including four intra-PLS pairs, J_1 , J_1' , J_2 , J_2' , and two equivalent inter-PLS pairs, J_{\perp}) and one next-nearest-neighbor (NNN) pair J_3 , marked in Figs. 3(a) and 3(b), plus three diagonal elements (A_i) of single-ion anisotropy matrix, are included to fit the dispersion. Using the fitting J values and the determined magnetic structure, the corresponding SW spectra $S(Q, E)$, along the four measured directions in the reciprocal space in units (H, K, L) are simulated as shown in Figs. 3(c)–3(f), which are in good agreement with the experimental data in Figs. 2(c)–2(f).

The important messages from the SW fitting and simulation are as follows: (1) The inter-PLS J_{\perp} , which characterizes the dispersion along the c axis, is less than 5% of the intra-PLS J_1 , J_1' , J_2 , J_2' , and J_3 , reflecting the quasi-2D magnetism. (2) Spins form AFM zigzag chains along the b axis due to the strong magnetic interactions J_1 and J_1' . These chains are coupled through the unexpected strong NNN interaction J_3 , comparable with J_1 and J_1' . (3) Within one PLS [see Fig. 3(b)], there are two distinct distorted triangles marked by gray (J_1, J_2 with J_3) and blue (J_1', J_2' with J_3), respectively. Although all the fitted J_{ij} values are positive, i.e., AFM, the spin configurations associated with J_2 and J_2' are FM [see Fig. 3(b)]; therefore, this lifts spin frustration within these triangles and leads to long-range magnetic order. (4) The anisotropic coefficients in the b and c directions are three orders larger than that in the a direction. This indicates that spins prefer to be aligned along the a axis with a collinear configuration. Such energetically more favorable state is obtained because of the 1D magnetoelastic effect [Fig. 1(c)]. The 1D magnetoelastic coupling along the a direction at T_N may be associated with the details of the exchange interaction [30,31]. In this case, J_3 needs to be large enough to stabilize such a magnetic structure against spin frustration in two triangular lattices. The magnetoelastic effect below T_N exactly reflects the correlation of J_3 and lattice constant in the a direction.

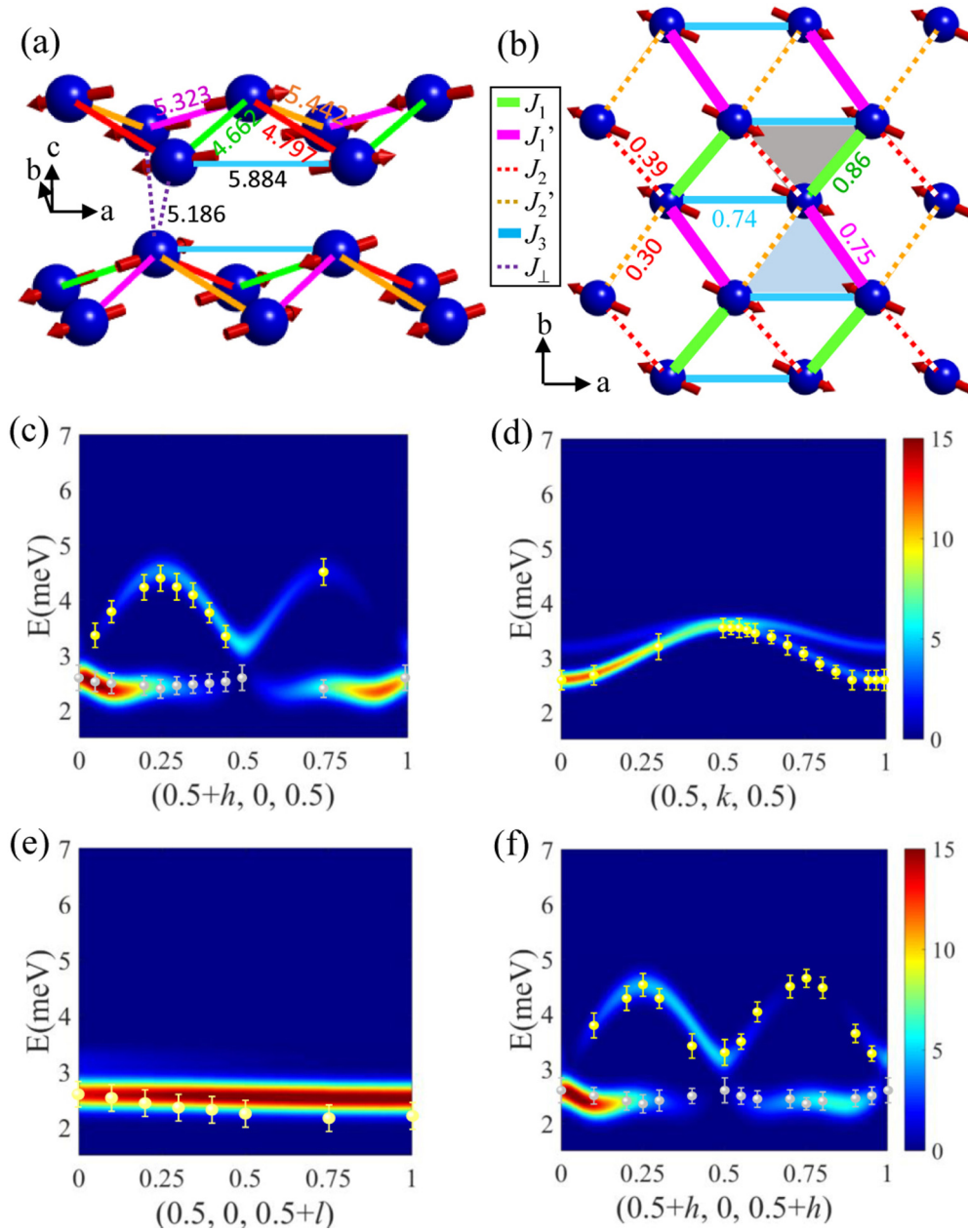


FIG. 3. (a) 3D illustration of Co-Co interaction network with spin configuration of two quasi-CoO₄ PLSs [see Fig. 2(b)] with the Co NN distances. (b) The *ab*-plane projection of one quasi-CoO₄ PLS showing Co-Co interactions, spin configurations with NN exchange parameters, buckled zigzag chains along the *b* axis, as well as the formed two triangular sublattices. (c)–(f) Simulated $S(Q, E)$ spectra along the $[H\ 0\ 0]$, $[0\ K\ 0]$, $[0\ 0\ L]$, and $[H\ 0\ H]$ directions in the r.l.u. using the magnetic exchange parameters obtained from the fits to the experimental SW dispersion and simulated intensity.

The quasi-2D magnetism in Ba₂CoO₄ is fundamentally different from the conventional quasi-2D magnetism compounds [2–6]: (i) The crystal structure is 3D with isolated CoO₄ tetrahedra, lacking well-separated magnetic and non-magnetic layers as in conventional quasi-2D magnetism compounds. (ii) There are two distinct stackings repeated along the *c* axis in Ba₂CoO₄. The spin arrangement is collinear within each stacking, but they are noncollinear between these two stackings connected by a negligible J_{\perp} to be responsible for the quasi-2D magnetism. (iii) Although intra-PLS Co-Co distance of J_{\perp} is shorter than those of the intra-PLS couplings

J'_1 , J'_2 , and J_3 , the magnitude of J_{\perp} between the two stackings is two orders smaller.

The static and dynamic magnetic behavior of magnetism in Ba₂CoO₄ is schematically summarized in Fig. 4(a): 1D spin-lattice coupling, quasi-2D spin waves, and 3D magnetic order. Given the fact that CoO₄ tetrahedra are isolated with large Co-Co spacing (>4.662 Å), there should be little direct exchange interaction between Co atoms. Thus, the spin-spin interaction via indirect spin-exchange pathways ought to be considered. For Ba₂CoO₄, indirect spin interactions may take place through Co-O···O-Co or Co-O-Ba-O-Co

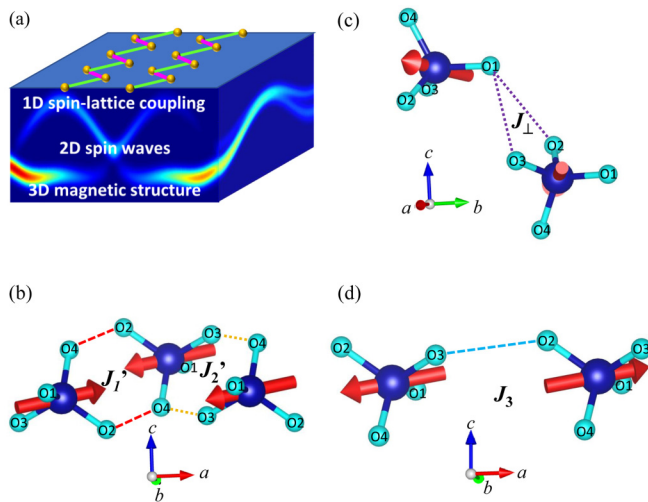


FIG. 4. (a) Illustrated view of different dimensional magnetism in Ba_2CoO_4 . The zigzag magnetic chains are schematically shown. Geometrical representation of indirect spin-exchange interaction paths of $\text{Co-O}\cdots\text{O-Co}$ associated with (b) inter-PLS NN interaction J_{\perp} , (c) intra-PLS NN interaction J_1' and J_2' , and (c), (d) intra-PLS NNN interaction J_3 in Ba_2CoO_4 .

exchange paths. The exchange path of $\text{Co-O}\cdots\text{O-Co}$ is referred to as the super-superexchange mechanism [16,19], in contrast to the conventional superexchange model [32]. The sign and the magnitude of interactions via $\text{Co-O}\cdots\text{O-Co}$ are not necessarily governed by the direct Co-Co distances, but by the overlap of orbitals along $\text{Co-O}\cdots\text{O-Co}$, especially the overlap of their p orbitals of the nonbonding $\text{O}\cdots\text{O}$ in the vicinity of the van der Waals distance [16–19]. Given that the $\text{O}\cdots\text{O}$ distances and the $\text{Co-O}\cdots\text{O}$ or $\text{O}\cdots\text{O-Co}$ angles are critical in determining the overlap of the $\text{O } p$ orbitals, it is important to compare the obtained magnetic exchange parameters with the corresponding crystallographic parameters. Thus, we determined the $\text{O}\cdots\text{O}$ distances and the $\text{Co-O}\cdots\text{O}$ or $\text{O}\cdots\text{O-Co}$ angles based on our Rietveld refinements of neutron-diffraction results. As shown in Figs. 4(b)–4(d) and Ref. [33], the inter-PLS Co-Co tetrahedra are less coplanar

than intra-PLS Co-Co tetrahedra, which does not favor the overlap of the $\text{O } p$ orbitals. In the two exchange pathways $\text{Co-O}_1\cdots\text{O}_3\text{-Co}$ and $\text{Co-O}_1\cdots\text{O}_2\text{-Co}$ for J_{\perp} [see Fig. 4(c)], the $\text{O}\cdots\text{O}$ distances are comparable to those for J_1', J_2' , and J_3 [see Figs. 4(b) and 4(d)], but the $\angle\text{Co-O}\cdots\text{O}$ and $\angle\text{O}\cdots\text{O-Co}$ angles are close to 90° and smaller than the corresponding angles for J_1', J_2' , and J_3 , thus leading to a much weaker J_{\perp} based on the SSE model (see Note 4 in Supplemental Material [34–36] for more details).

III. SUMMARY

In summary, we have investigated magnetic structure, magnetic interactions, and magnetoelastic coupling in Ba_2CoO_4 with isolated CoO_4 tetrahedra. The system exhibits a 3D non-collinear long-range AFM order below $T_N = 26$ K with magnetic moment primarily along the a axis. The spin-excitation spectra reveal a quasi-2D SW dispersion with an unusually large spin gap $\sim 2.55(3)$ meV, and the T -dependent lattice constants clearly illustrate a strong 1D magnetoelastic effect along the a axis. The concurrence of 3D lattice structure, 3D noncollinear magnetic structure, quasi-2D spin-waves dispersion, 1D magnetoelastic coupling, and the unusual intermediate spin state of Co^{4+} in a tetrahedral environment makes Ba_2CoO_4 a unique system for exploring magnetism. Our work may open an avenue to investigate quasi-2D magnetism in nonlayered structure involving isolated coordinate polyhedron and could be an important stimulus to explore the very rare intermediate spin state in the $3d^5$ cations such as Mn^{2+} , Fe^{3+} , and Co^{4+} in the tetrahedral environment.

ACKNOWLEDGMENTS

We would like to thank Zhentao Wang and Sándor Tóth for helpful discussions. This work was primarily supported by the US Department of Energy under EPSCoR Grant No. DE-SC0012432 with additional support from the Louisiana Board of Regents. Use of the high-flux isotope reactor at the Oak Ridge National Laboratory was supported by the US Department of Energy, Office of Basic Energy Sciences, Scientific User Facilities Division.

- [1] J. G. Bednorz and K. A. Müller, *Z. Phys. B* **64**, 189 (1986).
- [2] B. Keimer, S. A. Kivelson, M. R. Norman, S. Uchida, and J. Zaanen, *Nature (London)* **518**, 179 (2015).
- [3] Y. Kamihara, T. Watanabe, M. Hirano, and H. Hosono, *J. Am. Chem. Soc.* **130**, 3296 (2008).
- [4] T. J. Williams, A. A. Aczel, M. D. Lumsden, S. E. Nagler, M. B. Stone, J.-Q. Yan, and D. Mandrus, *Phys. Rev. B* **92**, 144404 (2015).
- [5] Q. Zhang, F. Ye, W. Tian, H. Cao, S. Chi, B. Hu, Z. Diao, D. A. Tennant, R. Jin, J. Zhang, and W. Plummer, *Phys. Rev. B* **95**, 220403(R) (2017).
- [6] S. Borisenko, D. Evtushinsky, Q. Gibson, A. Yaresko, T. Kim, M. N. Ali, B. Buechner, M. Hoesch, and R. J. Cava, [arXiv:1507.04847](https://arxiv.org/abs/1507.04847).
- [7] Von HJ. Mattausch and Hk. Muller-Buschbaum, *Z. Anorg. Allg. Chem.* **386**, 1 (1971).
- [8] K. Boulahya, M. Parras, A. Vegas, and J. M. González-Calbet, *Solid State Sci.* **2**, 57 (1998).
- [9] N. W. Ashcroft and N. D. Mermin, *Solid State Physics* (Holt, Rinehart and Winston, New York, 1976), p. 673.
- [10] K. Boulahya, M. Parras, J. M. González-Calbet, U. Amador, J. L. Martínez, and M. T. Fernández-Díaz, *Chem. Mater.* **18**, 3898 (2006).
- [11] R. Jin, H. Sha, P. G. Khalifah, R. E. Sykora, B. C. Sales, D. Mandrus, and J. Zhang, *Phys. Rev. B* **73**, 174404 (2006).
- [12] A. P. Ramirez, *MRS Bull.* **30**, 447 (2005).
- [13] A. A. Zvyagin, *Low Temp. Phys.* **39**, 901 (2013).

- [14] L. J. de Jongh and A. R. Miedema, *Adv. Phys.* **23**, 1 (1974).
- [15] P. L. Russo, J. Sugiyama, J. H. Brewer, E. J. Ansaldo, S. L. Stubbs, K. H. Chow, R. Jin, H. Sha, and J. Zhang, *Phys. Rev. B* **80**, 104421 (2009).
- [16] H.-J. Koo, K.-S. Lee, and M.-H. Whangbo, *Inorg. Chem.* **45**, 10743 (2006).
- [17] M.-H. Whangbo, D. Dai, and H.-J. Koo, *Solid State Sci.* **7**, 827 (2005).
- [18] M.-H. Whangbo, H.-J. Koo, and D. Dai, *J. Solid State Chem.* **176**, 417 (2003).
- [19] H.-J. Koo, M. H. Whangbo, and K.-S. Lee, *J. Solid State Chem.* **169**, 143 (2002).
- [20] See Supplemental Material at <http://link.aps.org/supplemental/10.1103/PhysRevB.99.094416> for details of experimental methods.
- [21] See Supplemental Material at <http://link.aps.org/supplemental/10.1103/PhysRevB.99.094416> for details of crystalline and magnetic structure determination with neutron diffraction.
- [22] B. C. Chakoumakos, H. Cao, F. Ye, A. D. Stoica, M. Popovici, M. Sundaram, W. Zhou, J. S. Hicks, G. W. Lynn, and R. A. Riedel, *J. Appl. Crystallogr.* **44**, 655 (2011).
- [23] P. Hidnert, *J. Res. Natl. Bur. Stand.* **52**, 311 (1954).
- [24] A. S. Wills, *Physica B* **276–278**, 680 (2000).
- [25] J. M. Perez-Mato, S. V. Gallego, E. S. Tasci, L. Elcoro, G. de la Flor, and M. I. Aroyo, *Annu. Rev. Mater. Res.* **45**, 217 (2015).
- [26] M. Pouchard, A. Villesuzanne, and J.-P. Doumerc, *C. R. Chim.* **6**, 135 (2003).
- [27] M. Kauffmann, O. Mentré, A. Legris, S. Hébert, A. Pautrat, and P. Roussel, *Chem. Mater.* **20**, 1741 (2008).
- [28] See Supplemental Material at <http://link.aps.org/supplemental/10.1103/PhysRevB.99.094416> for details of spin-wave dispersion determination.
- [29] S. Toth and B. Lake, *J. Phys.: Condens. Matter* **27**, 166002 (2015).
- [30] M. C. Cross and D. S. Fisher, *Phys. Rev. B* **19**, 402 (1979).
- [31] Y. Tokura, S. Seki, and N. Nagaosa, *Rep. Prog. Phys.* **77**, 076501 (2014).
- [32] P. W. Anderson, *Phys. Rev.* **79**, 350 (1950).
- [33] See Supplemental Material (Tables SIV and SV) at <http://link.aps.org/supplemental/10.1103/PhysRevB.99.094416> for details of interatomic distance, angles of the CoO₄ tetrahedra, and geometrical parameters of the SSE pathways.
- [34] See Supplemental Material at <http://link.aps.org/supplemental/10.1103/PhysRevB.99.094416> for details of possible magnetic exchange pathways.
- [35] R. Sinclair, H. D. Zhou, M. Lee, E. S. Choi, G. Li, T. Hong, and S. Calder, *Phys. Rev. B* **95**, 174410 (2017).
- [36] A. Möller, N. E. Amuneke, P. Daniel, B. Lorenz, C. R. de la Cruz, M. Gooch, and P. C. W. Chu, *Phys. Rev. B* **85**, 214422 (2012).